Proc. Natl. Acad. Sci. USA
Vol. 89, pp. 1271–1275, February 1992
Biochemistry

Fluorescence lifetime imaging of free and protein-bound NADH

JOSEPH R. LAKOWICZ*†, HENRYK SZMACINSKI*, KAZIMIERZ NOWACZYK*‡, AND MICHAEL L. JOHNSON§

*Center for Fluorescence Spectroscopy, Department of Biological Chemistry, University of Maryland School of Medicine, 660 West Redwood Street, Baltimore MD 21201; and §Department of Pharmacology, University of Virginia School of Medicine, Charlottesville, VA 22908

Communicated by Britton Chance, October 14, 1991 (received for review May 2, 1991)

ABSTRACT **We introduce a methodology, fluorescence lifetime imaging (FLIM), in which the contrast depends on the fluorescence lifetime at each point in a two-dimensional image and not on the local concentration and/or intensity of the fluorophore. We used FLIM to create lifetime images of NADH when free in solution and when bound to malate dehydrogenase. This represents a challenging case for lifetime imaging because the NADH decay times are just 0.4 and 1.0 ns in the free and bound states, respectively. In the present apparatus, lifetime images are created from a series of phase-sensitive images obtained with a gain-modulated image intensifier and recorded with a charge-coupled device (CCD) camera. The intensifier gain is modulated at the light-modulation frequency or a harmonic thereof. A series of stationary phase-sensitive images, each obtained with various phase shifts of the gain-modulation signal, is used to determine the phase angle or modulation of the emission at each pixel, which is in essence the lifetime image. We also describe an imaging procedure that allows specific decay times to be suppressed, allowing in this case suppression of the emission from either free or bound NADH. Since the fluorescence lifetimes of probes are known to be sensitive to numerous chemical and physical factors such as pH, oxygen, temperature, cations, polarity, and binding to macromolecules, this method allows imaging of the chemical or property of interest in macroscopic and microscopic samples. The concept of FLIM appears to have numerous potential applications in the biosciences.**

The phenomenon of fluorescence is widely utilized for research in the biosciences. These applications have been focused on two divergent types of measurements, time-resolved fluorescence and fluorescence microscopy. In the former, one takes advantage of the high information content of the time-dependent fluorescence decays to uncover details about the structure and dynamics of macromolecules (1–3). Such measurements are performed almost exclusively by using picosecond laser sources coupled with high-speed photodetectors. In contrast, fluorescence microscopy, in combination with dyes, stains, fluorophores, or fluorophore-labeled antibodies, is most often used to determine the localization of species of interest, usually proteins or other macromolecules (4–6). The acquisition of two-dimensional (2D) fluorescence images is typically accomplished with low-speed accumulating detectors. Consequently, the high information content of time-resolved fluorescence is not usually available for studies of microscopic biological samples. This is particularly disadvantageous when one considers the sensitivity of fluorescence decay times to chemical and environmental factors of interest, such as local pH, cation concentration, oxygen, and polarity, to name a few.

In the present report we combine measurements of fluorescence lifetimes with 2D imaging to create images in which the lifetimes at each pixel are used to create contrast in the images. While there have been reports of lifetime measurements at specific locations in microscopic samples (7–10), and in some cases the lifetime measurements have been raster-scanned to create crude lifetime images (11, 12), our approach is unique in that the lifetime information at each pixel is obtained simultaneously. Hence, the spatial resolution of the lifetime image will be ultimately limited by the optics and 2D detector rather than the time needed to measure the lifetime at each pixel. Importantly, our approach, in connection with advanced schemes for data acquisition and processing, should allow for nearly real-time display of lifetime images.

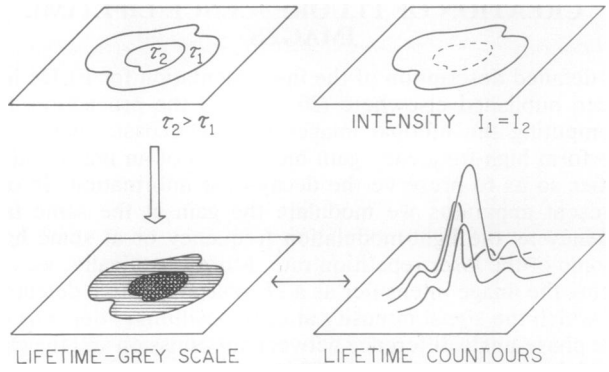

Scheme I. Intuitive description of FLIM.

The concept of fluorescence lifetime imaging (FLIM) is illustrated in Scheme I. Suppose the sample is composed of two regions, each with an equal fluorescence intensity. Assume further that the lifetime of the probe is several-fold higher in the central region of the object (τ_2) as compared with the larger outer region (τ_1). The longer lifetime in the central region could be due to the presence of a chemical species that increases the probe lifetime because of binding of the probe to a macromolecule or other environmental factors. The intensities of the central and outer regions could be equal because of dye exclusion or other mechanisms. Observation of the intensity image (Scheme I *Upper Right*) will not reveal the different environments in regions 1 and 2. However, if the lifetimes were measured, then the distinct environments would be detected. The FLIM method allows direct visualization of the spatially dependent decay times, which can be presented on a grey or color scale (Scheme I *Lower Left*) or as a three-dimensional (3D) projection in which the height represents the local decay time (Scheme I *Lower Right*). The concept of FLIM is an optical analogue of magnetic resonance imaging (MRI), in which the proton relaxation times at each location are used to create contrast in the calculated image.

The publication costs of this article were defrayed in part by page charge payment. This article must therefore be hereby marked "*advertisement*" in accordance with 18 U.S.C. §1734 solely to indicate this fact.

Abbreviations: FLIM, fluorescence lifetime imaging; CCD, charge-coupled device; 2D and 3D, two and three dimensional; POPOP, 1,4-bis[5-phenyl(oxazolyl)]benzene; MDH, malate dehydrogenase.

†To whom reprint requests should be addressed.
‡Permanent address: University of Gdańsk Institute of Experimental Physics, 80952 Gdańsk, Poland.

In the present report we describe the use of FLIM to image NADH when free in solution and when bound to a dehydrogenase. NADH was chosen because the emission of NADH from cells and tissues has been widely used for studies of the redox status of tissues (13–17), following the pioneering observations of Chance *et al.* (18) of the increase in NADH fluorescence under anoxic conditions. Additionally, resolution of free and bound NADH represents a challenging case for the FLIM methodology because the decay times are on the subnanosecond timescale (19).

CREATION OF FLUORESCENCE LIFETIME IMAGES

A detailed description of the instrumentation for FLIM has been published elsewhere (20), as will the procedures for computing the lifetime images (49). The basic idea is to perform high-frequency gain modulation of an image intensifier so as to preserve the decay-time information. In our present apparatus we modulate the gain at the same frequency as the light-modulation frequency or at some harmonic of the laser repetition rate. More specifically, we are using the image intensifier as a 2D phase-sensitive detector, in which the signal intensity at each position (r) depends on the phase-angle difference between the emission and the gain modulation of the detector. This results in a constant intensity that is proportional to the concentration of the fluorophore (C) at location r [$C(r)$], to the modulated amplitude of the emission at each pixel $m(r)$, and to the cosine of the phase-angle difference,

$$I(\theta_D, r) = kC(r)\left\{1 + \frac{1}{2} m_D m(r)\cos[\theta(r) - \theta_D]\right\}. \quad [1]$$

In this expression θ_D is the phase of the gain modulation, $\theta(r)$ is the phase angle of the fluorescence, and m_D is the gain-modulation degree. The phase angle of the emission at position r is related to the apparent phase lifetime $\tau_\theta(r)$ by

$$\tau_\theta(r) = \frac{1}{\omega}\tan\theta(r), \quad [2]$$

where ω is the light-modulation frequency in radians per second. The modulation of the emission at position r is related to the apparent modulation lifetimes $\tau_m(r)$ by

$$\tau_m(r) = \frac{1}{\omega}\left[\frac{1}{m^2(r)} - 1\right]^{1/2}. \quad [3]$$

The relationship between apparent phase and modulation lifetimes measured at a single modulation frequency and multiexponential decays has been widely discussed in the literature (21, 22). It is not possible to calculate the lifetime image from a single phase-sensitive image. However, the phase angle at each point in the image can be determined by examination of the detector phase-angle dependence of the image, which is easily accomplished by a series of electronic delays in the gain-modulation signal or by optical delays in the modulated excitation (20).

The desired information [$\theta(r)$ or $m(r)$] is thus obtained by varying θ_D (Eq. 1), which in turn allows calculation of $\tau_\theta(r)$ or $\tau_m(r)$. In our apparatus we collect a series of phase-sensitive images, in which θ_D is varied over 360 degrees or more. The phase-sensitive intensities at each pixel and detector phase angle are used to determine the phase and modulation at each pixel. This results in phase-angle, modulation, or lifetime images. The data sets for FLIM are rather large (512 × 512 pixels), which can result in time-consuming data storage, retrieval, and processing. To allow rapid calculations of images, we developed an algorithm that uses each image one time (49). In the present experiments, each phase-sensitive image was collected for 20 sec, so that a sequence of 10 phase-sensitive images can be obtained in 4 min or less. We were not attempting to use the highest available intensities, and in other experiments individual images are obtained in several seconds or less. The more time-consuming steps involve readout of the charge-coupled device (CCD) image (about 5 sec per image) and data processing. These steps can be accelerated in future instrumental configurations.

EXPERIMENTAL METHODS

The targets (Fig. 1) consisted of rows of cuvettes, each containing a standard fluorophore 1,4-bis[5-phenyl(oxazolyl)]-benzene (POPOP), NADH alone, or NADH with an excess of malate dehydrogenase (MDH). The laser passed through the center of the cuvettes. The light source is a picosecond dye laser system consisting of a mode-locked Antares NdYAG (neodymium/ythrium/aluminum-garnet laser), which synchronously pumps a cavity-dumped pyridine-1 dye laser, frequency-doubled to 355 nm. The pulse repetition rate was 3.7999 MHz. The emission was isolated from the excitation by using a Corning 3-75 filter, which transmits light >385 nm.

The detector was a CCD camera from Photometrics (series 200) with a thermoelectrically cooled PM-512 CCD. The gated image intensifier (Varo 510-5772-310) was positioned between the target and the CCD camera. The intensifier gain was modulated at 75.998 MHz by a rf signal applied between the photocathode and microchannel plate input surface (20). Phase delays were introduced into this gating signal by using calibrated coaxial cables. A somewhat more complex procedure was described previously by Feddersen *et al.* (23) for a linear CCD array.

Lifetime recovered from the FLIM measurements were compared with those obtained with standard frequency-domain measurements and instrumentation (24–26). For the FLIM measurements, polarizers were not used to eliminate the effects of Brownian rotation. NADH was obtained from Sigma and pig heart malate dehydrogenase was from Boehringer Mannheim, and both were dissolved in 100 mM Mops buffer (pH 7.0). The concentrations were 20 μM (HC) and 10 μM (LC) for NADH alone and 10 μM NADH with 20 μM MDH. POPOP was dissolved in undegassed cyclohexane. The temperature was room temperature, near 24°C.

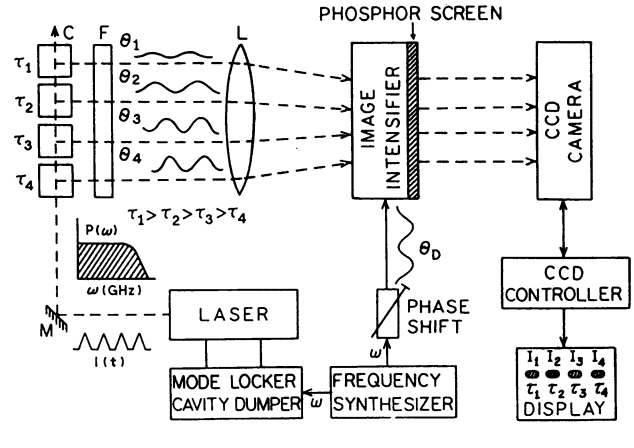

FIG. 1. Apparatus for FLIM. C boxes are cuvettes containing solutions with different lifetimes (τ) and different phase angles (θ).

RESULTS

Emission spectra of the test samples for FLIM are shown in Fig. 2. The structured emission is for POPOP, which was used as a reference fluorophore with an independently measured lifetime of 1.07 ns (Table 1). The emission from unbound NADH is unstructured with a maximum near 470 nm. Binding of NADH to MDH results in a 2-fold increase in the NADH intensity, which is typical for NADH binding to a dehydrogenase (27). We used two different solutions of NADH. In one (LC) the NADH concentration was identical to its concentration when bound to MDH. In the second, the NADH concentration was 2-fold larger (HC) to match the intensity of the MDH–NADH solution.

The lifetimes of these solutions were measured by using standard frequency-domain instrumentation (24–26) at a modulation frequency close to that used for the FLIM measurement (Table 1). The unequal phase and modulation lifetimes indicate that the NADH intensity decay is not singly exponential, as is known to be the case for free NADH (28).

The four solutions, three with NADH and one containing POPOP, were placed in four cuvettes and excited with the 355-nm laser beam as shown in Fig. 3. The phase-sensitive images were collected at a number of detector phase angles. Representative images are shown in Fig. 3 *Top* and *Middle*, which show the 2D images from the illuminated solutions and a tracing of the intensity measured for a line across the image. Also shown are 3D projections in which the horizontal plane represents the position and the height represents the phase-sensitive intensity. One notices that the phase-sensitive intensities are strongly dependent upon the detector phase angle.

The phase-sensitive intensities are expected to vary as the cosine of the detector phase angle (29, 30). In contrast to electronic phase-sensitive measurements (29, 30), negative optical intensities are not possible, and all intensities are greater than zero. The phase-sensitive intensities from the central illuminated region of each cuvette were fit to a cosine curve (Fig. 3 *Bottom*), and the resulting phase shifts are summarized in Table 1, in which the arbitrary detector phase angles of the apparatus (θ'_D) are corrected to absolute phase angles by using $\theta_D = \theta'_D - 201.8°$. This value was calculated by using the known phase angle and/or lifetime of POPOP. Inspection of the cosine curves in Fig. 3 *Bottom* reveals that

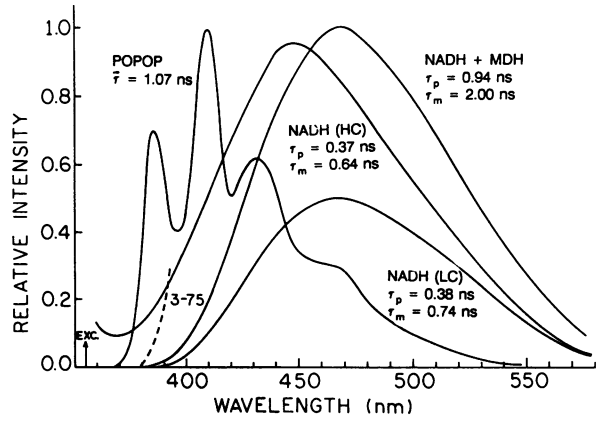

FIG. 2. Emission spectra of samples used for FLIM. The concentrations of NADH were 10 μM (LC) and 20 μM (HC) in the absence of MDH and 10 μM in the presence of 20 μM MDH.

the phase angles are nearly identical for the two solutions of unbound NADH. A larger phase shift was found for MDH-bound NADH, as is expected from the longer decay time (Table 1). The phase angle of POPOP is still larger because of its 1.05-ns lifetime. The phase angles from the central position in the phase-sensitive images are in good agreement with those obtained from the frequency-domain measurements (Table 1).

The phase-sensitive images, when collected over a range of detector phase angles, allow calculation of the phase angle and modulation at each pixel. Phase and modulation and lifetime images of the NADH solutions are shown in Fig. 4. The phase angle and lifetime of MDH-bound NADH is larger than that of free NADH seen on either side (Fig. 4 *Upper*). The larger phase angle is due to the longer lifetime of bound NADH. Similarly, the modulation of bound NADH is smaller than that of free NADH (Fig. 4 *Lower*). Note that the modulation scale is inverted to allow an upright lifetime scale. Such imaging, when applied to cellular systems, can provide a new basis for contrast based on the local biophysical and biochemical properties of the solutions.

Table 1. Phase, modulation, and lifetime data for NADH

Sample	Method*	Phase		Modulation	
		θ, deg	τ_θ,† ns	m	τ_m,† ns
NADH					
20 μM	FD	10.4	0.37	0.952	0.64
	Cosine	10.3 ± 6.0	0.38 ± 0.22	1.044 ± 0.15	0–1.03
	CCD FT	10.6 ± 1.0	0.36 ± 0.03	0.983 ± 0.01‡	0.38 ± 0.20
10 μM	FD	10.7	0.38	0.938	0.74
	Cosine	8.2 ± 7.8	0.30 ± 0.25	1.016 ± 0.18	0–1.38
	CCD FT	8.3 ± 0.8	0.29 ± 0.04	1.002 ± 0.09‡	0.46 ± 0.40
NADH + MDH	FD	24.2	0.94	0.710	2.0
	Cosine	18.4 ± 5.2	0.70 ± 0.21	0.822 ± 0.09	1.45 ± 0.50
	CCD FT	18.6 ± 1.5	0.68 ± 0.05	0.785 ± 0.03‡	1.70 ± 0.10
POPOP§	FD	26.6	1.05	0.885	1.10
				0.833‡	1.39

*FD indicates standard frequency-domain measurements at 79.695 MHz. Cosine refers to phase and modulation values obtained by least-squares fitting of the θ_D-dependent values, as shown in Fig. 3 *Bottom*. Typical uncertainties in the phase and modulation values are 0.2° and 0.005, respectively (25, 26). CCD FT refers to the pixel-by-pixel analysis (49).

†The uncertainty ranges of τ_θ and τ_m are not symmetrical, and average values are shown. For the cosine method, the uncertainties were from the usual assumptions in a least-squares fit. For the CCD FT calculations, the uncertainties in the standard value represent the standard deviations of about 50 pixels (5 × 10 pixels) from the central region of the illuminated spot.

‡A modulation of 0.833 for POPOP was used as reference modulation for CCD FT calculations (to obtain modulation lifetime for NADH larger than zero).

§POPOP in undegassed cyclohexane was used as reference sample.

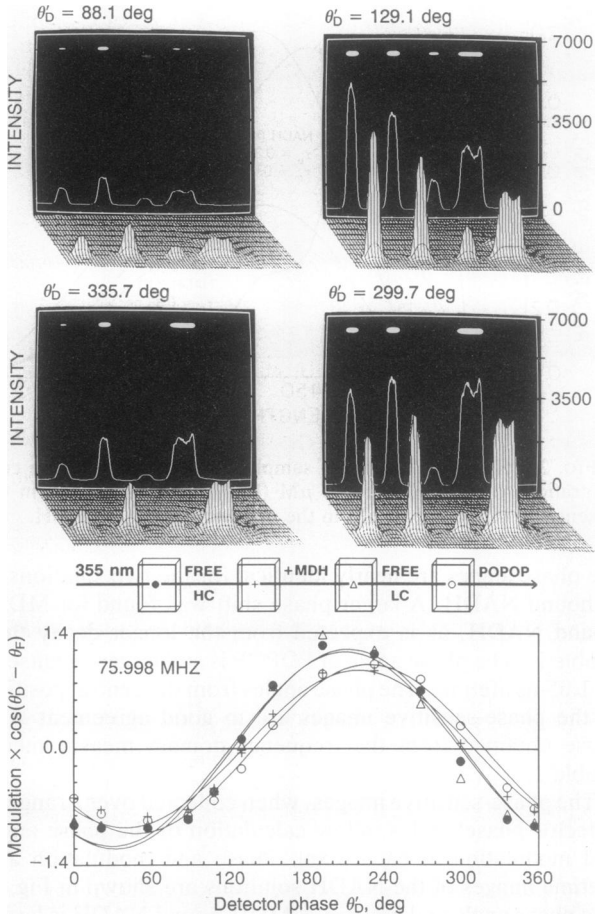

FIG. 3. (*Top* and *Middle*) Phase-sensitive fluorescence images of the four samples. (*Bottom*) Phase-sensitive intensities of the central illuminated region of each sample. ●, △, Two solutions of unbound NADH; +, MDH-bound NADH; ○, POPOP.

A unique property of FLIM is the ability to suppress the emission for any desired lifetime. This concept is shown schematically in Fig. 5. Suppression of any given decay time can be accomplished by taking the difference of two phase-sensitive images obtained for detector phase angles of θ_D and $\theta_D + \Delta$. In the difference image $\Delta I = I(\theta_D + \Delta) - I(\theta_D)$, components are suppressed ($\Delta I = 0$) with a specific decay time given by $\tau_0 = \omega^{-1} \tan(\theta_D + \Delta/2 \pm n180°)$. This concept is shown schematically in Fig. 5 for $\Delta = 180°$. Components with lifetimes larger than the suppressed lifetime appear as negative regions in the images, and components with shorter lifetimes have positive intensity. This relationship is reversed if one calculates $I(\theta_D) - I(\theta_D + \Delta)$. A more complete description of this suppression method will be presented elsewhere (49).

The use of difference images to suppress the emission of bound or free NADH is shown in Fig. 6, which shows the difference contours with positive and negative intensities. Also shown are the grey-scale images in which only the positive regions are shown as nonzero. In these grey-scale images, the negative regions were assigned zero intensity. Fig. 6*A* shows a positive nonprocessed phase-sensitive image in which all samples appear with nonzero intensity. In Fig. 6*B* the emission with a lifetime of 0.37 ns, close to that of free NADH, is suppressed, revealing a positive peak for bound NADH between the two free NADH samples. Similarly, in Fig. 6*C* the emission with lifetime of 0.47 ns is suppressed, revealing two positive images for free NADH on either side of the central sample of bound NADH, which appear as negative regions in the image.

This ability to selectively visualize free or bound NADH is of potential usefulness in studies of the redox state of tissues,

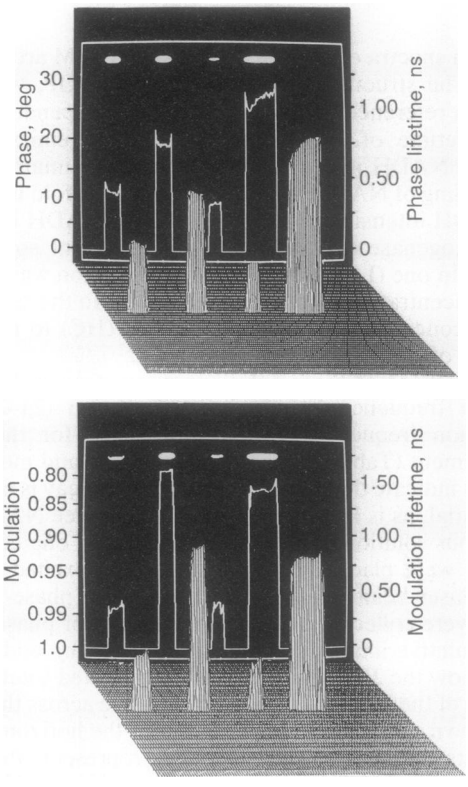

FIG. 4. Phase, modulation, and lifetime images of free and bound NADH.

where it may be informative to separately image free and bound NADH. Such procedures may provide a convenient method to obtain high-contrast images without resorting to the creation of a complete lifetime image.

DISCUSSION

FLIM provides an additional opportunity for the use of fluorescence in cell biology. This is because the lifetimes of probes can be sensitive to a variety of physical or chemical factors, many of which are of interest for studies of intracellular chemistry and physiology. The sensitivity of fluorescence lifetimes to chemical and physical properties of the local environment suggests that FLIM may be used for a variety of chemical imaging applications. We also note that

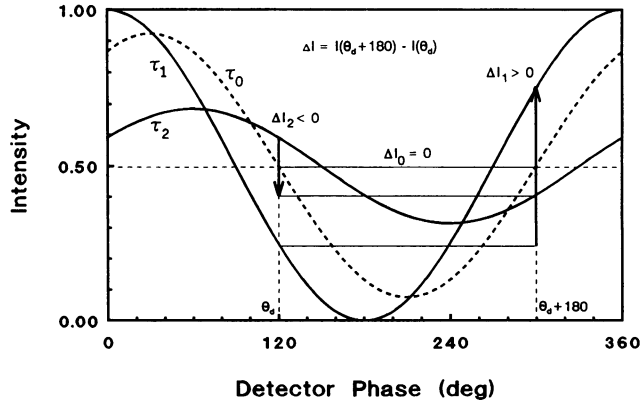

FIG. 5. Intuitive descriptions of phase suppression. In a difference image with $\Delta I = I(\theta_D + 180) - I(\theta_D)$, a component with $\theta = \theta_D$ is completely suppressed. Components with longer lifetimes (phase angles) appear as negative spots, and those with shorter lifetimes (phase angles) appear to be positive.

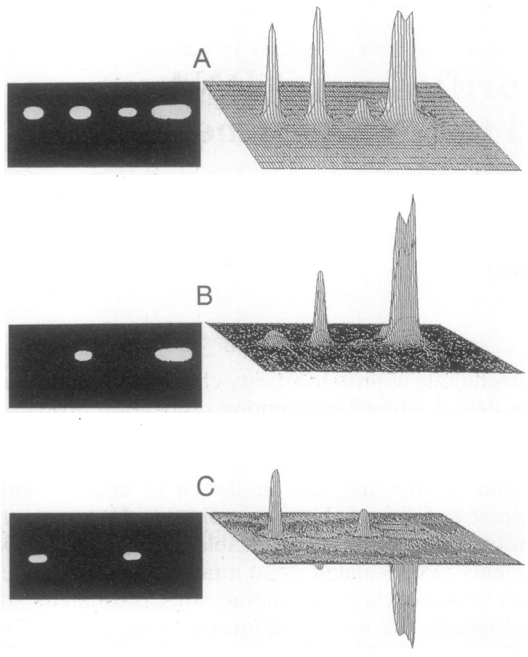

FIG. 6. Phase suppressed images of free and bound NADH. (*A*) Phase-sensitive image for θ_D° = 299.9°. (*B*) Difference image for $I(335.7°) - I(88.1°)$. The suppressed lifetime is 0.37 ns. (*C*) Difference image for $I(129.1°) - I(299.7°)$. The suppressed lifetime is 0.47 ns. In the grey-scale images, difference intensities < 0 are displayed as 0.

the present apparatus allows FLIM measurements at frequencies ranging from 1 to 150 MHz. Hence, one can readily conceive of multifrequency FLIM experiments in which a multiexponential decay is resolved at each pixel (unpublished data). Since the preexponential factors represent the relative amounts of the fluorophore present with each decay time, multifrequency FLIM may provide chemical imaging with quantitative information on partitioning of a probe between distinct local environments.

What types of chemical imaging can be accomplished with FLIM? At present, any such list will be incomplete because most fluorescence probes have been developed to display changes in wavelength or yield (31, 32) rather than lifetime. Nonetheless, it is known that the fluorescence lifetimes of probes can be altered by oxygen (33, 34), pH (35, 36), calcium (37, 38), energy transfer (39–41), and a variety of other factors and/or quenchers (9, 42–47). To date, most fluorescence sensors have not been characterized by lifetime measurements, and it is probable that such data will reveal additional probes that are useful for FLIM measurements. It will also be of interest to examine lifetime images of stained chromosomes (46), where the local G-C/A-T ratios may affect the decay times of the stains (9). Such imaging could rely on the wealth of knowledge of the fluorescent properties of dye–DNA complexes (47).

Furthermore, fluorescence lifetimes are mostly independent of the probe concentration, at least for the low concentrations and/or thin samples used for microscopy. Also, FLIM images are likely to be insensitive to photobleaching. These two factors suggest that given a suitable fluorophore, the lifetime at each pixel can reveal details about the local chemical composition of cellular and/or microscopic samples. And finally we note that the components required for FLIM are commonly used in fluorescence microscopy, including the preferred CCD detector (48). The main expense of implementing FLIM measurements will be use of frequency synthesizers, amplifiers and a modulated light source, which should decrease with advances in laser technology and the use of long-wavelength fluorophores.

We thank Dr. Badri Maliwal for assistance in preparation of the MDH-NADH samples. We acknowledge support from grants from the National Science Foundation (DIR-8710401 and DMB-8804931) and support from the Medical Biotechnology Center at the University of Maryland, without whose support these experiments could not have been accomplished.

1. Lakowicz, J. R., ed. (1990) *Proc. SPIE* **1204.**
2. Jameson, D. M. & Reinhart, G. (1989) *Fluorescent Biomolecules* (Plenum, New York).
3. Demchenko, A. P. (1986) *Ultraviolet Spectroscopy of Proteins* (Springer, Berlin).
4. Taylor, D. L., ed. (1989) *Fluorescence Microscopy of Living Cells in Culture* (Academic, New York), Part A.
5. Taylor, D. L. & Wang, Y., eds. (1989) *Fluorescence Microscopy of Living Cells in Culture* (Academic, New York), Part B.
6. Wilson, T., ed. (1990) *Confocal Microscopy* (Academic, New York).
7. Keating, S. M. & Wensel, T. G. (1990) *Proc. SPIE*, **1204**, 42–48.
8. Bottiroli, G., Cionini, P. G., Docchio, F. & Sacchi, C. A. (1984) *Histochem. J.* **16**, 223–233.
9. Arndt-Jovin, D. J., Latt, S. A., Striker, G. & Jovin, T. M. (1979) *J. Histochem. Cytochem.* **27**, 87–95.
10. Herman, B. A. & Fernandez, S. M. (1978) *J. Cell. Physiol.* **94**, 253–264.
11. Wang, S. F., Kitajima, S., Uchida, T., Coleman, D. M. & Minami, S. (1990) *Appl. Spectrosc.* **44**, 25–30.
12. Wang, X. F., Uchida, T. & Minami, S. (1989) *Appl. Spectrosc.* **43**, 840–845.
13. Masters, B. R., Ghosh, A. K., Wilson, J. & Matschinsky, F. M. (1989) *Invest. Ophthalmol. Vis. Sci.* **30**, 861–868.
14. Koretsky, A. P., Katz, L. A. & Balaban, R. S. (1987) *Am. J. Physiol.* **253**, H856–H262.
15. Avi-Dor, Y., Olson, J. M., Doherty, M. D. & Kaplan, N. O. (1962) *J. Biol. Chem.* **237**, 2377–2383.
16. Salmon, J. M., Kohen, E., Viallet, P., Hirschberg, J. G., Wouters, A. W., Kohen, C. & Thorell, B. (1982) *Photochem. Photobiol.* **36**, 585–593.
17. Chance, B. & Lieberman, M. (1978) *Exp. Eye Res.* **26**, 111–117.
18. Chance, B., Legallais, V. & Schoener, B. (1962) *Nature (London)* **195**, 1073–1076.
19. Scott, T. G., Spencer, R. D., Leonard, N. J. & Weber, G. (1970) *J. Am. Chem. Soc.* **92**, 687–695.
20. Lakowicz, J. R. & Berndt, K. W. (1991) *Rev. Sci. Instrum.* **62**, 1727–1734.
21. Spencer, R. D. & Weber, G. (1969) *Ann. N.Y. Acad. Sci.* **158**, 361–376.
22. Jameson, D. M. & Weber, G. (1981) *J. Phys. Chem.* **85**, 953–958.
23. Feddersen, B., Gratton, E., Glegg, R. M. & Jovin, T. (1990) *Biophys. J.* **59**, 155a (abstr.).
24. Lakowicz, J. R. & Maliwal, B. P. (1985) *Biophys. Chem.* **21**, 61–78.
25. Lakowicz, J. R., Laczko, G. & Gryczynski, I. (1986) *Rev. Sci. Instrum.* **57**, 2499–2506.
26. Laczko, G., Lakowicz, J. R., Gryczynski, I., Gryczynski, Z. & Malak, H. (1990) *Rev. Sci. Instrum.* **61**, 2331–2337.
27. Anderson, S. R. & Weber, G. (1965) *Biochemistry* **4**, 1948–1957.
28. Visser, A. J. W. G. & vanHoek, A. (1981) *Photochem. Photobiol.* **33**, 35–40.
29. Cherek, H. & Lakowicz, J. R. (1981) *J. Biochem. Biophys. Methods* **5**, 19–35.
30. Lakowicz, J. R. & Cherek, H. (1981) *J. Biol. Chem.* **256**, 6348–6353.
31. Komada, H., Nakabayashi, H., Nakano, H., Hara, M., Yoshida, T., Takanari, H. & Izutsu, K. (1989) *Cell Struct. Funct.* **14**, 141–150.
32. Grynkiewicz, G., Poenie, M. & Tsien, R. Y. (1985) *J. Biol. Chem.* **260**, 3440–3450.
33. Kautsky, H. (1930) *Trans. Faraday Soc.* **35**, 216–219.
34. Lakowicz, J. R. & Weber, G. (1973) *Biochemistry* **12**, 419–423.
35. Laws, J. R. & Brand, L. (1979) *J. Phys. Chem.* **83**, 795–802.
36. Gafni, A. & Brand, L. (1978) *Chem. Phys. Lett.* **58**, 346–350.
37. Keating, S. M. & Wensel, T. G. (1991) *Biophys. J.* **59**, 186–202.
38. Miyoshi, N., Hara, K., Shiro, K., Nakanishi, K. & Fukuda, M. (1991) *Photochem. Photobiol.* **53**, 415–418.
39. Förster, Th. (1948) *Ann. Phys. (Leipzig)* **2**, 55–75 (translated by R. S. Knox).
40. Stryer, L. (1978) *Annu. Rev. Biochem.* **47**, 819–846.
41. Steinberg, I. Z. (1971) *Annu. Rev. Biochem.* **40**, 83–114.
42. Eftink, M. R. & Ghiron, C. (1981) *Anal. Biochem.* **114**, 199–227.
43. Lehrer, S. S. (1971) *Biochemistry* **10**, 3254–3263.
44. Ware, W. R., Watt, D. & Holmes, J. D. (1974) *J. Am. Chem. Soc.* **96**, 7853–7860.
45. Leto, T. L., Roseman, M. A. & Holloway, P. W. (1980) *Biochemistry* **19**, 1911–1916.
46. Weisblum, B. & de Haseth, P. L. (1971) *Proc. Natl. Acad. Sci. USA* **69**, 629–632.
47. Steiner, R. F. & Kubota, Y. (1983) in *Exited State of Biopolymers*, ed. Steiner, R. F. (Plenum, New York), pp. 203–254.
48. Hiraoko, Y., Sedat, J. W. & Agard, D. A. (1987) *Science* **238**, 36–41.
49. Lakowicz, J. R., Szmacinski, H., Nowaczyk, K. & Johnson, M. L. (1992) *Anal. Biochem.*, in press.